Type-I spontaneous parametric down-conversion with a strongly focused pump

H. Di Lorenzo Pires, F. M. G. J. Coppens, and M. P. van Exter*
Huygens Laboratory, Leiden University, P.O. Box 9504, 2300 RA Leiden, The Netherlands
(Received 24 December 2010; published 31 March 2011)

We experimentally study the spatial properties of the field generated by spontaneous parametric down-conversion (SPDC) when the pump laser beam is strongly focused in the nonlinear crystal. Special attention is paid to classical intensity measurements with a CCD camera. We introduce the concept of a classical equivalent source that replicates all the coherence properties of SPDC light and explains all our experimental results. We show that, in contrast with experiments with a well-collimated pump, here both the phase-matching conditions and the position of the focusing plane determine the measured intensity profiles in the image plane of the crystal. The transition from the near-field regime to the far field is investigated. Measurements of two-photon correlations under strong focusing are also presented and the special features thereof are discussed.

DOI: 10.1103/PhysRevA.83.033837 PACS number(s): 42.65.Lm, 42.50.Dv, 03.67.Mn

I. INTRODUCTION

Spontaneous parametric down-conversion (SPDC) is a nonlinear optical process in which some photons from a laser beam can effectively be split into two lower frequency photons [1–6]. The theoretical model of down-conversion of light belongs to the domain of quantum optics, which is necessary to explain the highly nonclassical photon statistics exhibited by the generated photons. Indeed, if one tries to understand the SPDC process within the classical optics paradigm, one will be stumped by the following observation. A completely coherent laser beam generates, after interacting with a crystal, a highly incoherent beam which still has a very special spatial distribution. Figure 1(a) shows a typical measurement of a far-field intensity profile. The so-called SPDC ring is very incoherent, but at the same time seems to be a clear signature of a coherent process. What is then the origin of the resulting randomness? A solution to this difficulty is to admit that coherence should be preserved, but in the form of a high-order coherence. Such a generalization was introduced by Glauber in his prestigious "quantum theory of optical coherence" [7]. He realized that the classical concept of coherence was no longer adequate to the needs of various experiments at that time. In the context of SPDC, one recognizes nowadays the so-called *two-photon field* which is endowed with high-order coherence but lacks low-order coherence, that is, where the two-photon state is pure while the reduced one-photon state is mixed. This observation is closely related to the concept of *entanglement* [8–12]. Had the modes not been entangled, the field would be coherent in all orders.

Naturally, there are many different regimes in which one can produce down-converted light. Both the coherence and the spatial shape of the emitted field depend on the pump shape and on the phase-matching conditions. In the most popular configuration, a well-collimated laser beam is used to pump the nonlinear crystal. In this regime the emission is highly incoherent and both the near-field and far-field intensities have been extensively studied. Figure 1(a) shows the far-field intensity pattern observed in this regime. Due to the small momentum spread in the initial beam, the SPDC ring at a fixed emission frequency is very narrow, indicating the conservation of transverse momenta. A near-field image under the same conditions only reveals the spatial profile of the pump laser, in this case a Gaussian. Note that these considerations apply to *classical* intensity measurements with a CCD camera. More interesting structures are revealed in the near field for correlations measured by two scanning detectors [13,14]. For an excellent review on the quantum aspects of the spatial correlations in SPDC see Ref. [15].

More recently, the effect of strongly focused pumping on SPDC has been considered [16–27]. For type-II down-conversion, focusing has been shown to create an asymmetric broadening of the far-field rings [19,21]. For type-I SPDC, the effect is illustrated in Fig. 1(b). We see that a large momentum spread in the initial beam causes a broadening of the ring as a larger set of transverse momenta can now be phase matched. It has also been demonstrated how the coupling of down-converted photons into optical fibers can be enhanced by properly focusing the pump beam [17,25–27]. Not much attention has been paid, however, to the shape of the emission in the near field (or image plane) of the crystal, which is the topic of this paper.

In this work we study the spatial structure of type-I down-converted light generated by a highly focused Gaussian beam. In particular, we explore the rich structures that appear in the image plane of the crystal. Surprisingly, in the transition from plane wave to focused pumping the near-field intensity profiles reveal an extremely rich and yet unexplored structure. Most of this work concentrates on the *classical* intensity patterns that can be measured by a CCD camera. Contrary to the far field, where only the phase-matching conditions and the divergence of the pump determine the intensity patterns, the near-field patterns strongly depend on the exact focusing plane. The use of a focused pump is also interesting because in this regime the down-converted light can be almost coherent. In this way it will be possible to observe the transition from the near field to the far field as would be expected from a Fourier relationship.

Since most of our experiments are classical, it is tempting to describe the results with a theoretical model that is as classical as possible. In this context we have developed a simple model that allows us to compute the coherence function

*mvexter@molphys.leidenuniv.nl

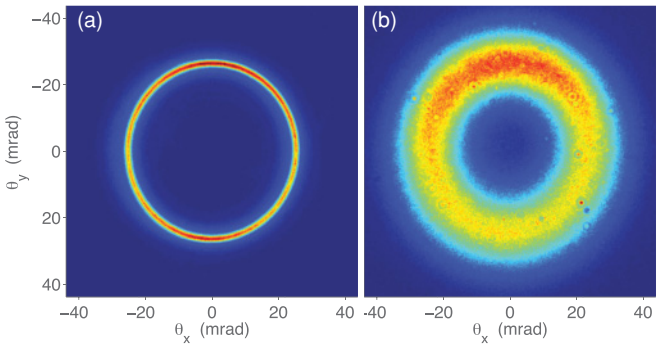

FIG. 1. (Color online) Typical far-field intensity profiles for type-I SPDC measured for (a) collimated pump and (b) strongly focused pump.

of the down-converted light. More specifically, we obtain the *classical equivalent source*, which is sufficient to explain our measurements. We also show that these predictions agree with those from the standard SPDC model based on a two-photon field.

This article is organized as follows. In Sec. II we present a theoretical formulation of the problem and calculate the coherence function of the generated field. In Sec. III we introduce our experimental setup and present results of near-field intensity measurements. For comparison, we present in Sec. IV measurements of two-photon correlations and discuss our experiments in the context of the well-known two-photon wave function. A summary of our results and conclusions are presented in Sec. V.

II. CLASSICAL EQUIVALENT SOURCE OF PARAMETRIC DOWN-CONVERSION

The standard quantum model of spontaneous parametric down-conversion consists of writing the Hamiltonian of the interaction of the pump with the nonlinear crystal and calculating the evolution of the initial state by expanding the time evolution operator in a power series [1–6]. The initial state is considered to be the vacuum state plus a classical coherent pump. The final state will also contain photon pairs, traditionally called *single* and *idler*, whose spatial and spectral distributions are completely described by the obtained two-photon wave function. If one is interested not in two-photon correlations but in the single-photon properties, one can obtain the reduced one-photon state by a partial trace, that is, integrating over all possible modes of the other photon.

Many experiments on SPDC do not directly probe the quantum aspects of two-photon correlations, but instead use single detectors to measure the spatial and spectral properties of the emitted field. Is it possible to explain the outcomes of such measurements without the detour via a two-photon state? In other words, is there a semiclassical model to explain those classical results? It is known that SPDC, within the classical coherence paradigm, can be described as a three-wave mixing process between the pump beam and quantum vacuum fluctuations, which is now the only nonclassical element in the description [28,29]. Specially in this context, where one interprets the generated field as a parametric amplification of noise fluctuations, SPDC is also known as *parametric fluorescence*.

The usual route to describe the spatial and spectral pattern formation in parametric fluorescence consists of writing the governing differential equations of the field in the nonlinear medium, including a stochastic term representing the vacuum noise [30,31]. The problem of the origin of coherence in parametric fluorescence has been the subject of investigation and the outcome depends crucially on the experimental conditions. For a plane-wave pump, it has been argued that walk-off is the key ingredient for the onset of coherence [32], while in the focused regime, "spatial mode locking" is the responsible mechanism [33]. It has also been shown that in the spatiotemporal domain the emission has a special skewed structure [34–36]. Many of the theoretical models behind these phenomena are quite involved and numerical simulations are usually required to illustrate the underlying physics.

Below we introduce a model that sheds light on the origin of coherence in SPDC for different focusing and phase-matching conditions. Although very simple, it provides the exact working equations in the sense that it equals those obtained via a partial trace of the complete two-photon field (see Sec. IV). We will restrict the analysis to describe our measurements of near-field intensities of frequency-degenerate type-I SPDC generated by a cw pump, but it can, in principle, be extended to more general cases.

Figure 2 shows the geometry considered in the calculations. A Gaussian laser beam is initially focused inside a nonlinear crystal of length L. The Rayleigh range inside the crystal is $z_p = \frac{1}{2}k_p w_p^2$, where k_p is the pump wave number and w_p is the beam waist. In order to clarify the theoretical description and simplify the equations we will first assume that the right-hand side of the crystal, which is our region of interest, is embedded in a medium with the same refractive index n, but without nonlinearities. The consequences of refraction for the real experiment will be discussed later on.

The essence of nonlinear optical phenomena is the coupling of two waves yielding a response at a different frequency. We are interested in down-converted light at a frequency ω for a pump frequency $\omega_p = 2\omega$. Our model consists of assuming that each point inside the crystal emits down-converted light driven by the source term $E_p(\boldsymbol{r}')\xi^*(\boldsymbol{r}')$, which describes the coupling of the pump field to the quantum noise fluctuations at position $\boldsymbol{r}'$. The observed field $A(\boldsymbol{r})$ is just the sum of all contributions propagated to the observation point $\boldsymbol{r}$, namely,

$$A(\boldsymbol{r}) = \int_{\text{crystal}} d\boldsymbol{r}'\; E_p(\boldsymbol{r}')\xi^*(\boldsymbol{r}')\mathcal{G}(\boldsymbol{r}-\boldsymbol{r}'). \tag{1}$$

The propagator $\mathcal{G}(\boldsymbol{r}-\boldsymbol{r}')$ is, in our case, the Green function of the paraxial wave equation, which assumes the form [37]

$$\mathcal{G}(\boldsymbol{r}-\boldsymbol{r}') = \frac{k\, e^{ik(z-z')}}{2\pi i(z-z')} \exp\left[\frac{ik|\boldsymbol{\rho}-\boldsymbol{\rho}'|^2}{2(z-z')}\right], \tag{2}$$

where we express the position $\boldsymbol{r} = (\boldsymbol{\rho}, z)$ in polar coordinates and $k = n(\omega)\omega/c$ is the wave number at the desired frequency ω.

The coherence properties of the generated field can be obtained by an ensemble average and is described by the coherence function $W(\boldsymbol{r}_1,\boldsymbol{r}_2) = \langle A^*(\boldsymbol{r}_1)A(\boldsymbol{r}_2)\rangle$. The signal (or

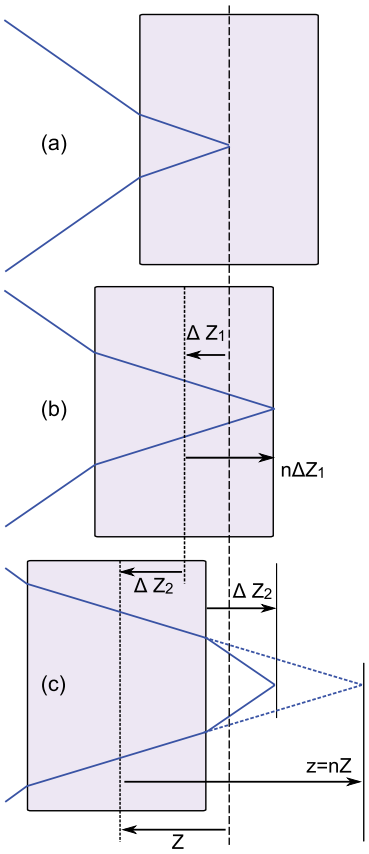

FIG. 2. (Color online) Geometry considered in our calculations and measurements. (a) A Gaussian beam is strongly focused in the center of a nonlinear crystal. (b) Pump focused inside the crystal. A crystal displacement ΔZ_1 corresponds to a focus displacement $n\Delta Z_1$ with respect to the center of the crystal (we show the extreme case). (c) Pump focused outside the crystal. An extra crystal displacement ΔZ_2 beyond the point where the pump focus is located at the back facets brings the pump focus the same distance ΔZ_2 behind this facet. In the theoretical description we assume that the output of the crystal is embedded in a medium of refractive index n, so that the pump focus is always located at a distance $z = nZ$ from the center of the crystal, as shown with the dashed (blue) lines.

idler) mode is initially in the vacuum state $|0\rangle$. One can show that the expected value of the coherence in the vacuum state is given by

$$\langle \xi^*(\boldsymbol{r})\xi(\boldsymbol{r}')\rangle = \mathcal{G}(\boldsymbol{r}-\boldsymbol{r}'). \tag{3}$$

This crucial result is a consequence of the unequal-time commutation relation of the electric field operator $[E(\boldsymbol{r},t),E^\dagger(\boldsymbol{r}',t')] = G(\boldsymbol{r},\boldsymbol{r}';t-t')$, where G is the time-dependent Green function. It is proven, for instance, in Ref. [38] and implies that $\langle 0|EE^\dagger|0\rangle = G$. By expressing the Green function in the frequency domain via a Fourier transform [39,40], we can select the desired spectral component of $\mathcal{G}$ and obtain Eq. (3). With those ingredients, it is easy to show that the coherence of the SPDC field is given by

$$W(\boldsymbol{r}_1,\boldsymbol{r}_2) = \iint_{\text{crystal}} d\boldsymbol{r}'d\boldsymbol{r}''\; W_s(\boldsymbol{r}',\boldsymbol{r}'')\mathcal{G}^*(\boldsymbol{r}_1-\boldsymbol{r}')\mathcal{G}(\boldsymbol{r}_2-\boldsymbol{r}''), \tag{4}$$

where

$$W_s(\boldsymbol{r}',\boldsymbol{r}'') = E_p^*(\boldsymbol{r}')E_p(\boldsymbol{r}'')\mathcal{G}(\boldsymbol{r}'-\boldsymbol{r}''). \tag{5}$$

We can interpret these equations as follows. Equation (4) is nothing more than the coherence between the points $\boldsymbol{r}_1$ and $\boldsymbol{r}_2$ due to a volumetric source of partially coherent light. The source field W_s is propagated to the observation points using two Green functions $\mathcal{G}$. The exact shape of the source is given by Eq. (5), which we consider as the *classical equivalent source* of SPDC. It means that a volumetric element with the dimensions of the crystal, emitting light with a initial coherence described by Eq. (5), replicates all classical properties of the SPDC light. The appearance of the term $\mathcal{G}(\boldsymbol{r}'-\boldsymbol{r}'')$, instead of $\delta(\boldsymbol{r}'-\boldsymbol{r}'')$ as one would expect from a pure fluorescent source, is a consequence of the coupling of the pump to the vacuum fluctuations. It is this term that makes parametric fluorescence different.

In order to measure the z dependence of the field, we will translate the crystal longitudinally. Figure 2 shows how refractive effects affect the results. We call Z the physical displacement of the crystal. In Fig. 2(b) we see that while the pump is still focused inside the crystal a displacement ΔZ_1 of the crystal corresponds to a displacement $n\Delta Z_1$ of the focus with respect to the center of the crystal. The reason is that, upon entering a dielectric medium, a paraxial Gaussian beam retains its waist but is stretched in the longitudinal direction by a factor n. On the other hand, when the pump is focused outside the crystal [as in Fig. 2(c)] an extra crystal displacement ΔZ_2 correspond now to a focus displacement of also ΔZ_2. In our simplified model, in which the output of the crystal is embedded in a medium of refractive index n, the pump focus is always located at a distance $z = nZ$ from the center of the crystal. Experimentally, the field at the plane z, which contains the beam waist, is imaged with a lens onto a CCD camera. By moving the nonlinear crystal we change the relative position of the focus with respect to the center of the crystal, in effect probing the longitudinal dependence of the field. It is important to remark that whether the pump is focused inside the crystal or outside the lens will always image the pump focus. In other words, we always have a "sharp" image of the focus plane independent of the position of the crystal. This holds both for the real experiment and for our simplified theoretical description. The effect of such an imaging scheme can be mathematically described in our model by propagating the source field to the plane nZ. Considering the explicit form of the pump beam

$$E_p(\boldsymbol{\rho},z) \propto \frac{e^{ik_pz}}{z-nZ-iz_p}\exp\left[\frac{ik_p\rho^2}{2(z-nZ-iz_p)}\right], \tag{6}$$

the SPDC near-field intensity $I(\boldsymbol{r}) = W(\boldsymbol{r},\boldsymbol{r})$ can be calculated using Eqs. (2)–(6). After integrating the Gaussian functions and performing some additional manipulations, we find

$$I(\boldsymbol{\rho},Z) \propto \int_{-L/2-nZ}^{L/2-nZ} dz' \int_{-L/2-nZ}^{L/2-nZ} dz'' \frac{e^{-i\Delta k(z'-z'')}}{z_p(z'-z'')-2iz'z''} \times \exp\left[\frac{-2k\rho^2(z'-z'')}{z_p(z'-z'')-2iz'z''}\right], \tag{7}$$

where $\Delta k = k_p - 2k$ is the on-axis wave vector mismatch. $I(\boldsymbol{\rho}, Z)$ is the intensity that we measure with a CCD camera when the crystal is at position Z. In order to interpret Eq. (7), it is useful to rewrite it in a different form. One can show that

$$I(\boldsymbol{\rho}, Z) \propto \int_{-\infty}^{+\infty} d\boldsymbol{\rho}' |V(\boldsymbol{\rho} - \boldsymbol{\rho}', Z)|^2 e^{-(\boldsymbol{\rho}+\boldsymbol{\rho}')^2/2w_p^2} \tag{8}$$

with

$$V(\boldsymbol{\rho}, Z) = \int_{-L/2-nZ}^{L/2-nZ} dz' \, \frac{e^{-i\Delta k z'}}{z'} e^{ik\rho^2/4z'}. \tag{9}$$

From Eq. (8) we see that for a tightly focused pump the intensity $I(\boldsymbol{\rho}) \to |V(2\boldsymbol{\rho}, Z)|^2$. Equation (8) is expressed as a convolution where the Gaussian profile of the pump beam acts as a smoother. As we will show in Sec. IV, Eqs. (8) and (9) are identical to the equations obtained via the standard approach based on the two-photon field. Here we have shown that the same results can be obtained without such a detour. We will also demonstrate that Eq. (9) is simply the Fourier transform of a propagated sinc-type phase-matching function. It is interesting to notice that for a well collimated pump beam the *far-field* profile is well described by a "sinc". For a strongly focused pump beam it is the *near-field* intensity that can be describe by (the Fourier transform of) the sinc. In the next section we will present measurements performed in the strongly focused regime.

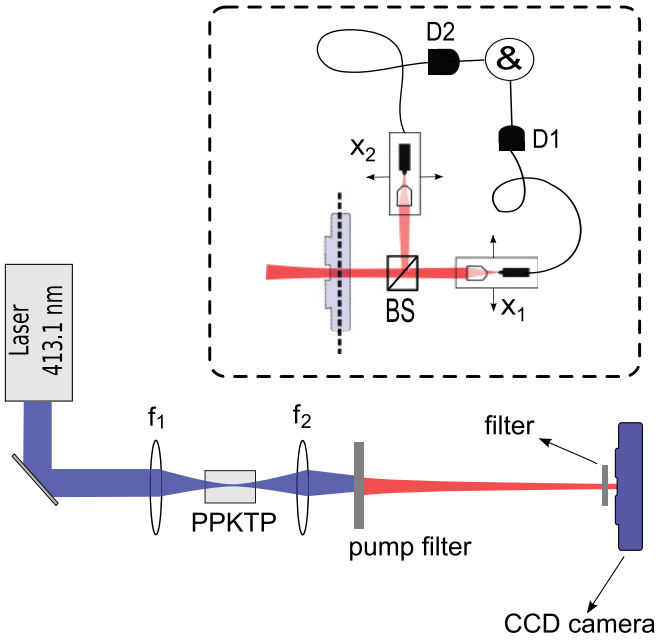

FIG. 3. (Color online) Experimental setup used to generate SPDC light and to measure the intensity pattern in the image plane of the crystal. Lens $f_1 = 100$ mm focuses the pump to a $w_p = 11$ μm spot size and lens $f_2 = 59$ mm makes a $10\times$ magnified image of the pump focus plane onto a CCD camera. The crystal can be longitudinally translated. The inset shows a modified detection scheme used to measure two-photon correlations, as discussed in Sec. IV.

III. NEAR-FIELD INTENSITY MEASUREMENTS

The purpose of our experiments is to explore the near-field intensity profiles of light generated by SPDC under strong focusing and observe the transition between near and far field in the regime of almost coherent emission.

Figure 3 shows the experimental setup. A $L = 20$-mm long periodically polled $KTiOPO_4$ crystal (PPKTP) is pumped by a 50 mW krypton-ion laser beam operating at 413.1 nm, generating SPDC light. A $f_1 = 100$ mm lens is used to focus the pump laser to a $w_p = 11$ μm spot size. These experimental parameters satisfy the paraxial wave approximation assumed in the theoretical description. The crystal is mounted on a translation stage that allows it to be moved longitudinally along the focal region. The distance between the center of the crystal and the beam is depicted in Fig. 2. A second lens $f_2 = 59$ mm is used to make a $10\times$ magnified image of the plane where the pump beam is focused onto a CCD camera (Apogee Alta U1). A narrow band spectral filter ($\Delta\lambda = 5$ nm at $\lambda = 826.2$ nm) is used to select light close to frequency degeneracy.

We first investigate the near-field intensity patterns for different phase-matching conditions and different longitudinal positions Z of the nonlinear crystal. For our type-I PPKTP, the on-axis phase mismatch $\varphi = \frac{1}{2}\Delta k L$ depends approximately linearly on the crystal temperature and can therefore be conveniently adjusted. The derivative $d\varphi/dT = (4.0 \pm 0.3)$ K^{-1} has been experimentally obtained. For our measurements we choose a certain phase mismatch φ and scan the longitudinal position of the crystal. For each position we take a picture with the CCD camera. The results shown next are built by taking a horizontal (x) cross section of each of these figures and positioning them next to each other. In other words, we show the dependence of the *intensity cross sections* $I(x, Z)$ versus the Z position of the crystal. Owning to the rotational symmetry of the images measured by the CCD, we are in effect fully characterizing the near-field intensity $I(\boldsymbol{\rho}, Z)$.

Figure 4 shows the experimental and theoretical results for four different values of the phase mismatch φ. Different acquisition times were used for these pictures in order to compensate for the change in total power with phase matching. The overall photon flux $F(\varphi)$ relative to its $\varphi = 0$ value is given by $F(\varphi)/F(0) = 1 + (2/\pi)[\varphi \mathrm{sinc}^2\varphi - \mathrm{Si}(2\varphi)]$, where $\mathrm{Si}(x) = \int_0^x \mathrm{sinc}\, x' \, dx'$ is the sine integral function. This dependence has been checked experimentally. A curve fitting of $F(\varphi)$ revealed to be a very reliable method to determine the temperature $T_0 = (60.76 \pm 0.02)^\circ$C for perfect phase matching and the aforementioned derivative $d\varphi/dT$. The dashed white lines in the theoretical plots show the positions $Z = \pm L/2n$, where the pump focus coincides with the crystal facets.

Figures 4(a) and 4(e) correspond to $\varphi = -7.0$ being associated with open far-field SPDC rings and more efficient conversion. Figures 4(b) and 4(f) correspond to perfect phase matching, that is, $\varphi = 0$. Figures 4(c) and 4(g) for $\varphi = 1.0$ and Figs. 4(d) and 4(h) for $\varphi = 2.6$ are associated with closed far-field SPDC rings and inefficient emission.

We can interpret the results as follows. While the pump beam is focused in a plane *inside* the crystal, the intensity profiles are bounded to a limited range $|x| \lesssim 40$ μm. The dashed lines indicate the facets of the crystal which are spaced by $\Delta Z = L/n = 11.6$ mm. As predicted by Eqs. (8) and (9), the results are symmetric with respect to the $Z = 0$ plane. The

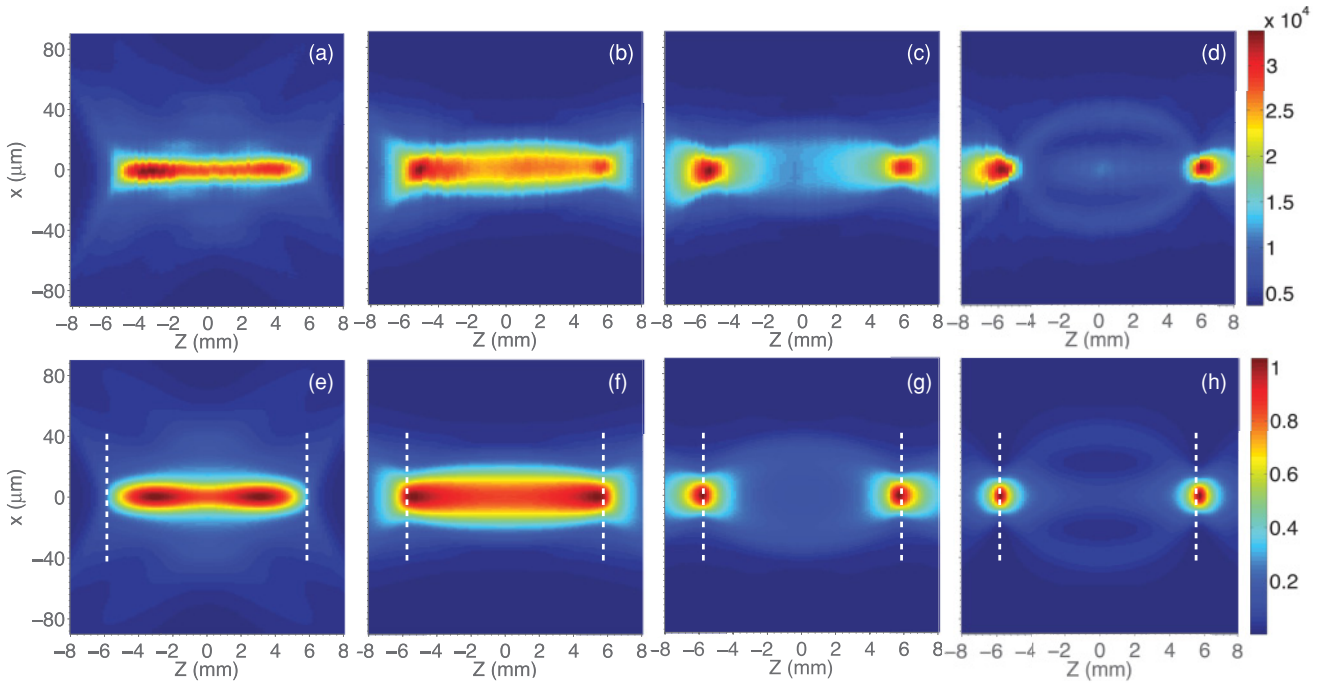

FIG. 4. (Color online) Measured (upper row) and calculated (lower row) cross sections of the near-field SPDC intensity patterns as a function of the longitudinal position Z of the crystal. Results for four different values of the phase mismatch are shown, namely, (a, e) $\varphi = -7.0$, (b, f) $\varphi = 0.0$, (c, g) $\varphi = 1.0$, and (d, h) $\varphi = 2.6$. The dashed white lines in the theoretical plots show the positions $Z = \pm L/2n$, where the pump focus coincides with the crystal facets.

profiles are thus identical if one focuses the pump on either side of the crystal. For $\varphi \leqslant 0$ the width of the distribution is approximately constant and depends only slightly on Z. The curves are narrower for more negative values of φ. For $\varphi > 0$ there is a more noticeable position dependence. When the beam waist coincides with either facets of the crystal, the near-field intensity has a very pronounced central peak. All other focusing planes lead to a broader intensity distribution. Figure 4(d) shows, for instance, that when the beam is focused in the center of the crystal, three small but wide peaks are observable. This redistribution of energy is such that the total power $P = \int I(\rho, Z) 2\pi\rho \, d\rho$ is conserved. The reason is that the total SPDC yield depends only on the divergence of the pump beam, which is constant throughout the experiment. All structures observed in Fig. 4 are a consequence of the diffraction integrals which can be quite interesting [as in Fig. 4(d)]. The transition of an axial valley to an axial peak in near-field imaging also appears, for instance, in the context of Fresnel diffraction. By changing the initial phase structure of the field, many different diffraction patterns can be observed. Here the phase-matching conditions strongly determine this phase structure.

Figure 5 shows the measured cross sections of intensity patterns taken for Z values corresponding to the transition from the near to the far field. For clarity, the square root of the measured intensities is shown. The four figures correspond to (a) $\varphi = -15.0$, (b) $\varphi = -7.0$, (c) $\varphi = 3.0$, and (d) $\varphi = 9.0$. We made the horizontal axis of Figs. 5(a) and 5(b) different from Figs. 5(c) and 5(d) because for $\varphi < 0$ the transition from the near field to the far field occurs for $Z \approx 6$ mm $\approx L/2n$, while for $\varphi > 0$ the far field begins for $Z \approx 8$ mm $> L/2n$. This can also be seen in Fig. 4. Since the pump beam is focused outside the crystal, the horizontal axis which represents the crystal displacement is now equal to the displacement of the

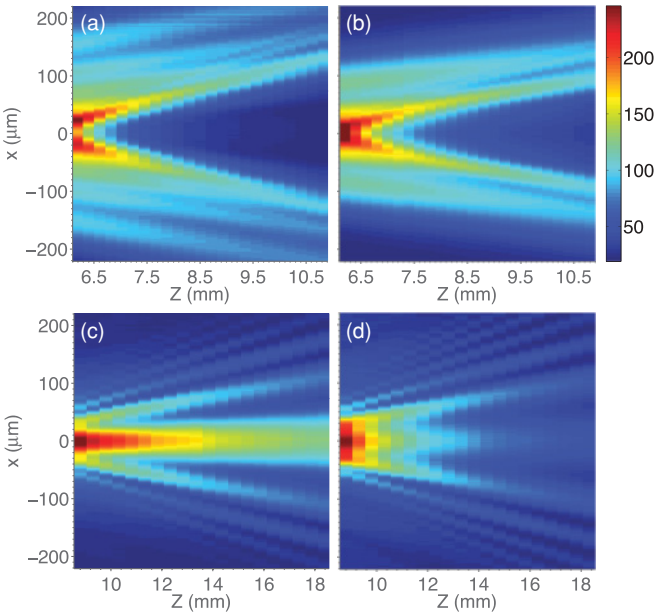

FIG. 5. (Color online) Measured cross sections of the intensity patterns in the transition region between the near field and the far field. The square root of the measured intensity is shown in a false color scale. The figures correspond to the following phase-mismatch parameters: (a) $\varphi = -15.0$, (b) $\varphi = -7.0$, (c) $\varphi = 3.0$, and (d) $\varphi = 9.0$.

pump focus from the back facet plus $L/2n$ (see remarks in Sec. II).

We see that all transverse intensity profiles in Fig. 5 are clearly a function of angle only, expanding under propagation without gaining new structures. Figures 5(a) and 5(b) correspond to open far-field SPDC rings ($\varphi < 0$); the radius of the ring is proportional to $\sqrt{|\varphi|}$. Figures 5(c) and 5(d) correspond to closed rings ($\varphi > 0$), but the typical patterns of nonphase matched SPDC can still be recognized.

The theoretical predictions, calculated with the formalism of Sec. II, agree very well with the experimental results. Those results are the measurements of Eq. (8) in the intensity patterns of SPDC. This function has only been measured in the correlations between the two photons [14] in a weak focusing geometry. We have shown now that by using a strongly focused pump these patterns can also be detected with a CCD camera.

It might come as a surprise that we are able to observe detailed spatial structures both in the near-field images (Fig. 4) and in the far-field type images obtained after sufficient propagation (Fig. 5). This is possible only because our source is not completely incoherent, but instead still contains a considerable degree of coherence. The number of generated modes at perfect phase matching ($\varphi = 0$) and with the pump focused at the center of the crystal ($Z = 0$) depends on a single, dimensionless parameter $b\sigma = \sqrt{L/2z_p}$. In both limits $b\sigma \to 0$ and $b\sigma \gg 1$ the number of generated modes is very large and the emission is almost incoherent [9]. When $b\sigma \approx 1$ the number of modes is close to unity and the field is almost coherent. For our experiments, $b\sigma = 2.5$, meaning that some coherent effects at the single-photon level can still be observed, like the approximate Fourier relation between the near and far field. This can be physically understood as follows. The patterns measured in Fig. 4 are described by the Fourier transform $\mathcal{F}$ of a sinc function, propagated and convoluted with a narrow Gaussian. The narrower the pump, the more the profiles approach $\mathcal{F}$(sinc). On the other hand, the far-field patterns shown in Fig. 5 are qualitatively described by a sinc function. The rings are somewhat thicker, though, due to the divergence of the pump beam. The less divergent the pump is, the more the far-field resembles a sinc. Only in the intermediate, almost-coherent regime ($b\sigma \approx 1$, corresponding to a "narrow, but not too divergent" beam) one will be able to observe the approximate Fourier relation between near and far fields.

IV. NEAR-FIELD TWO-PHOTON CORRELATIONS

The results presented so far can be explained by the semiclassical model of Sec. II. In this section we will show how our measurements can equally well be understood in terms of the well-know entangled two-photon field model of parametric down-conversion. Furthermore, we will present experimental evidence of entanglement migration between the amplitude and the phase of the field.

The so-called *two-photon field* $\tilde{A}(\boldsymbol{q}_1,\boldsymbol{q}_2)$ is a complex valued function that gives the probability amplitude of finding one photon with transverse momentum $\boldsymbol{q}_1$ and the other photon with transverse momentum $\boldsymbol{q}_2$. In the absence of walk-off, this function has a special form factorizing in two functions of the sum and difference momenta as [15]

$$\tilde{A}(\boldsymbol{q}_1,\boldsymbol{q}_2) = \tilde{E}_p(\boldsymbol{q}_1 - \boldsymbol{q}_2)\ \mathrm{sinc}\left(\frac{L}{4k_p}|\boldsymbol{q}_1 - \boldsymbol{q}_2|^2 + \varphi\right), \tag{10}$$

where $\tilde{E}_p$ is the angular spectrum of the pump beam with wave number k_p, L is the crystal thickness and φ is the on-axis phase mismatch, as defined in Sec. II.

In order to describe measurements in the near field, that is, in the image plane of the crystal, the wave function should be written in spatial coordinates, which is obtained by combining a Fourier transform from momenta $\boldsymbol{q}$ to positions $\boldsymbol{\rho}$ with a propagation to the desired z plane. One can show that the spatial representation of the two-photon field also factorizes as

$$A(\boldsymbol{\rho}_1,\boldsymbol{\rho}_2;z) = E_p\left(\frac{\boldsymbol{\rho}_1 + \boldsymbol{\rho}_2}{2},z\right) V(\boldsymbol{\rho}_1 - \boldsymbol{\rho}_2,z). \tag{11}$$

The function V is exactly the same as the one defined by Eq. (9) and E_p is the spatial profile of the pump beam. The coincidence rate measured by two detectors at positions $\boldsymbol{\rho}_1$ and $\boldsymbol{\rho}_2$ is $R_{cc} \propto |A|^2$. The "classical" intensity measured by one single detector can be obtained by a partial trace, that is, integrating over all possible positions of the other detector such that $I(\boldsymbol{\rho},z) \propto \int |A(\boldsymbol{\rho},\boldsymbol{\rho}_2;z)|^2 d\boldsymbol{\rho}_2$. We now recover Eq. (8) that describes our experimental results. Again an extremely focused pump would act as a "delta function", making the measured intensity $I(\boldsymbol{\rho},Z) \propto |V(2\boldsymbol{\rho},Z)|^2$.

So far we have studied intensity measurements. In the regime we are operating, however, special features also appear in the two-photon correlations. We will now discuss one particular interesting result. In order to measure those correlations we use the modified setup shown in the inset of Fig. 3. The ICCD camera is removed and the image plane is now re-imaged with objectives onto the input tips of two single-mode optical fibers which are then connected to photon counting modules. A beam splitter is used to separate the two photons; coincidences counts are post selected by an electronic circuit.

Figure 6 shows the measured coincidence rate when both detectors are scanned horizontally at a phase mismatch $\varphi = 3.2$. Due to the rotational symmetry of Eq. (11) we are basically mapping the function $|A(x_1,x_2;Z_0)|^2$, where x_1 and x_2 are transverse positions of detectors 1 and 2, respectively. The crystal is placed at two different longitudinal positions (a) $Z_0 = 0$, in which the pump is focused at center of the crystal, and (b) $Z_0 = L/2n$, in which the focus coincides with the crystal facet.

In Fig. 6(a) the two-photon field is clearly nonseparable, that is, $A(x_1,x_2) \neq f(x_1)g(x_2)$. Two distinct patterns can be observed in the sum $x_1 = x_2$ and difference coordinates $x_1 = -x_2$. Those diagonals cross sections are also plotted on the right side of Fig. 6. When $x_1 = x_2$ we measure the pump profile which is nonlocally transferred to the correlations in the term E_p. When $x_1 = -x_2$ we observe the function V which characterizes the phase-matching conditions. In the regime of strong focusing, the coincidences are very compact in the diagonal $x_1 = x_2$ and extended in the diagonal $x_1 = -x_2$. Note that these combinations are opposite to those observed in

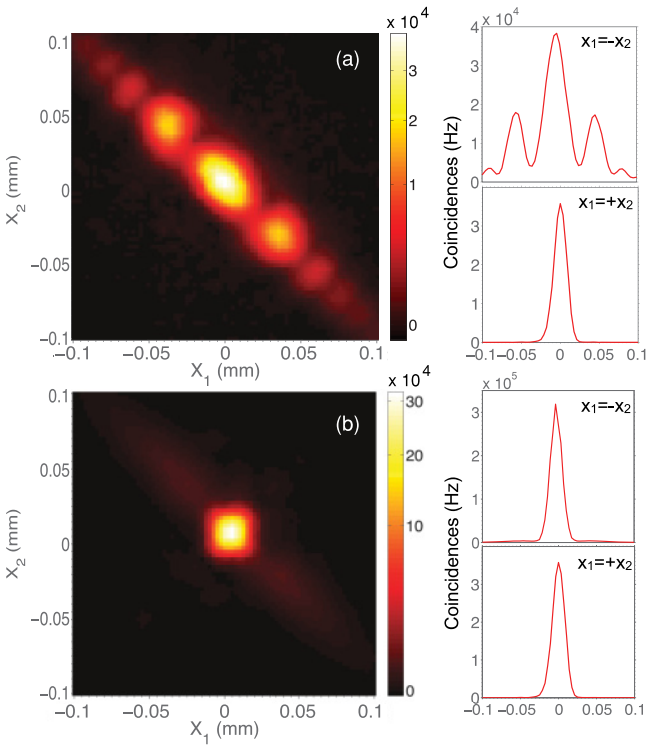

FIG. 6. (Color online) Coincidences rate as measured by two scanning detectors with transverse positions x_1 and x_2. The phase mismatch parameter is set to $\varphi = 3.2$ and the pump beam is focused (a) at the center of the crystal and (b) at the crystal facet. Diagonal scans for $x_1 = x_2$ and $x_1 = -x_2$ are also shown.

the weak focusing regime. As we have argued, measurements with a CCD camera show nothing more than a horizontal projection of this pattern.

Observing Fig. 6(b), where the pump is focused at the crystal facet, one might erroneously conclude that the two-photon field is separable, that is, nonentangled. The pattern is almost circular and the cross sections in the sum and difference coordinates have approximately the same width. However, when the pump is focused at the facet the amount of entanglement, as measured by the Schmidt number K [9], is actually predicted to be higher. The dependence of the number of entangled modes with the focusing plane is nontrivial and has not yet been extensive studied. By following a procedure similar to the one proposed in [9,41] we can verify, however, that K increases when the pump is focused at the crystal facet. The reason of this apparent discrepancy is that correlations exist not only between the amplitude of the two photons, but also between their phases. When the amplitude correlations are minimal, all the entanglement has migrated to the phase of the field [42]. This illustrates the importance of phase entanglement.

V. CONCLUSION

In this work we have experimentally studied how strongly focusing of the pump beam shapes the field generated by spontaneous parametric down-conversion. Special attention was paid to yet unexplored near-field intensity measurements. We have shown that the collinear phase mismatch and the pump focusing plane are the most important variables in determining the measured intensity profiles. We developed a semiclassical model that can explain our measurements via the parametric amplification of vacuum fluctuations. In this way we obtained a classical equivalent source that is able to mimic all the coherence properties of SPDC light. The equations are in agreement with those obtained via the standard quantum model of SPDC. We have experimentally studied the transition of the intensity distributions from the near field to the far field. The near-field regime extends to a range of the length of the nonlinear crystal, from this point on the SPDC rings start to acquire shape. Finally, we have presented measurements of two-photon correlations under strong focusing. Signatures of amplitude and phase entanglement were discussed. Our results provide new insights into the nature of SPDC emission under strong focusing and have potential applications in experiments where spatial aspects of down-conversion are relevant.

ACKNOWLEDGMENTS

The authors acknowledge W. H. Peeters for useful discussions. This work has been supported by the "Stichting voor Fundamenteel Onderzoek der Materie (FOM)" and by the EU under the FET-Open Agreement "HIDEAS", No. FP7-ICT-221906.

[1] B. R. Mollow, Phys. Rev. A **8**, 2684 (1973).
[2] D. N. Klyshko, Sov. J. Quantum Electron. **7**, 591 (1977).
[3] C. K. Hong and L. Mandel, Phys. Rev. A **31**, 2409 (1985).
[4] L. Mandel and E. Wolf, *Optical Coherence and Quantum Optics* (Cambridge University Press, Cambridge, 1995).
[5] Z. Y. J. Ou, *Multi-Photon Quantum Interference* (Springer, New York, 2007).
[6] T. B. Pittman, D. V. Strekalov, D. N. Klyshko, M. H. Rubin, A. V. Sergienko, and Y. H. Shih, Phys. Rev. A **53**, 2804 (1996).
[7] R. J. Glauber, Phys. Rev. **130**, 2529 (1963).
[8] B. E. A. Saleh, A. F. Abouraddy, A. V. Sergienko, and M. C. Teich, Phys. Rev. A **62**, 043816 (2000).
[9] C. K. Law and J. H. Eberly, Phys. Rev. Lett. **92**, 127903 (2004).
[10] J. C. Howell, R. S. Bennink, S. J. Bentley, and R. W. Boyd, Phys. Rev. Lett. **92**, 210403 (2004).
[11] S. P. Walborn and C. H. Monken, Phys. Rev. A **76**, 062305 (2007).
[12] H. DiLorenzo Pires, C. H. Monken, and M. P. van Exter, Phys. Rev. A **80**, 022307 (2009).
[13] H. Di Lorenzo Pires and M. P. van Exter, Phys. Rev. A **79**, 041801(R) (2009).
[14] H. Di Lorenzo Pires and M. P. van Exter, Phys. Rev. A **80**, 053820 (2009).
[15] S. P. Walborn, C. H. Monken, S. Pádua, and P. H. Souto Ribeiro, Phys. Rep. **495**, 87 (2010).

[16] R. Andrews, E. Pike, and S. Sarkar, Opt. Express **12**, 3264 (2004).
[17] A. Dragan, Phys. Rev. A **70**, 053814 (2004).
[18] D. Ljunggren and M. Tengner, Phys. Rev. A **72**, 062301 (2005).
[19] P. S. K. Lee, M. P. van Exter, and J. P. Woerdman, Phys. Rev. A **72**, 033803 (2005).
[20] G. Molina-Terriza, S. Minardi, Y. Deyanova, C. I. Osorio, M. Hendrych, and J. P. Torres, Phys. Rev. A **72**, 065802 (2005).
[21] R. S. Bennink, Y. Liu, D. D. Earl, and W. P. Grice, Phys. Rev. A **74**, 023802 (2006).
[22] A. Ling, A. Lamas-Linares, and C. Kurtsiefer, Phys. Rev. A **77**, 043834 (2008).
[23] Ö. Süzer and T. Goodson, Opt. Express **16**, 20166 (2008).
[24] Z. Zhao, K. A. Meyer, W. B. Whitten, R. W. Shaw, R. S. Bennink, and W. P. Grice, Phys. Rev. A **77**, 063828 (2008).
[25] P. Kolenderski, W. Wasilewski, and K. Banaszek, Phys. Rev. A **80**, 013811 (2009).
[26] R. S. Bennink, Phys. Rev. A **81**, 053805 (2010).
[27] L. E. Vicent, A. B. UÕRen, R. Rangarajan, C. I. Osorio, J. P. Torres, L. Zhang, and I. A. Walmsley, New J. Phys. **12**, 093027 (2010).
[28] W. H. Louisell, A. Yariv, and A. E. Siegman, Phys. Rev. **124**, 1646 (1961).
[29] A. Yariv, *Quantum Electronics* (Wiley, New York, 1989).
[30] B. Schröder, Opt. Quantum Electron. **15**, 57 (1983).
[31] A. Gatti, H. Wiedemann, L. A. Lugiato, I. Marzoli, G. L. Oppo, and S. M. Barnett, Phys. Rev. A **56**, 877 (1997).
[32] A. Picozzi and M. Haelterman, Phys. Rev. E **63**, 056611 (2001).
[33] P. Di Trapani, G. Valiulis, W. Chinaglia, and A. Andreoni, Phys. Rev. Lett. **80**, 265 (1998).
[34] A. Picozzi and M. Haelterman, Phys. Rev. Lett. **88**, 083901 (2002).
[35] O. Jedrkiewicz, A. Picozzi, M. Clerici, D. Faccio, and P. Di Trapani, Phys. Rev. Lett. **97**, 243903 (2006).
[36] O. Jedrkiewicz, M. Clerici, A. Picozzi, D. Faccio, and P. Di Trapani, Phys. Rev. A **76**, 033823 (2007).
[37] H. F. Schouten and T. D. Visser, Am. J. Phys. **76**, 867 (2008).
[38] M. W. Mitchell, Phys. Rev. A **79**, 043835 (2009).
[39] G. Bimonte, J. Phys. A: Math. Theor. **43**, 155402 (2010).
[40] W. Eckhardt, Phys. Rev. A **29**, 1991 (1984).
[41] N. Gonzalez, G. Molina-Terriza, and J. P. Torres, Phys. Rev. A **80**, 043804 (2009).
[42] K. W. Chan, J. P. Torres, and J. H. Eberly, Phys. Rev. A **75**, 050101(R) (2007).